Journal of the European Ceramic Society 44 (2024) 4536–4548

Contents lists available at ScienceDirect

Journal of the European Ceramic Society

journal homepage: www.elsevier.com/locate/jeurceramsoc

Processing and oxidation resistance at 1650 °C of ZrB_2-based UHTCMCs with short fibre gradients

Matteo Mor, Antonio Vinci *, Diletta Sciti

CNR-ISSMC, Institute of Science, Technology and Sustainability for Ceramics, Via Granarolo 64, 48018 Faenza, RA, Italy

ARTICLE INFO

Keywords:
Ultra-high-temperature ceramic matrix composites (UHTCMC)
Gradient structures
ZrB_2
$MoSi_2$
Oxidation resistance

ABSTRACT

Functionally graded composites with fibre gradients were prepared with three different ceramic matrices: ZrB_2-SiC-Y_2O_3, ZrB_2-$MoSi_2$ and SiC-Y_2O_3, with short carbon fibres in amounts ranging from 0–50%. Short term oxidation tests at 1650 °C in air were carried out to study the influence of the graded architecture and fibre content on the structural stability and oxidation resistance. The composite layers were perfectly joined at the interface, with no visible defects. Even after oxidation testing, no spallation phenomena were observed. ZrB_2-$MoSi_2$ matrix proved to be the most effective in protecting the composite from oxidation thanks to the formation of a compact ZrO_2-SiO_2 scale.

1. Introduction

Ultra-high-temperature ceramics (UHTCs) are a class of materials that include carbides and borides of early transition metals, characterized by a melting point above 3000 °C [1,2]. They are widely recognized for their high thermal conductivity and exceptional ablation resistance in harsh environments [3]. However, UHTC materials are characterized by poor fracture toughness, which leads to catastrophic failure and limits their application in environments where thermal shocks and vibrations are present [4]. To improve the damage tolerance of the UHTCs, short or long fibres have been considered as a reinforcement [5–7]. Among the different fibres, carbon fibres have shown the best resistance at high energy fluxes, provided they are well protected by the UHTC matrix and sintered using processes that do not affect the fibre properties [8–10]. Another approach to improving the failure resistance of ceramics is to exploit the stresses that arise from the layering of different compositions with different properties [11–14]. The main challenges in a multi-layered structure can be the residual stresses resulting from differences in thermal expansion coefficient, Young's modulus, chemical reactions, and phase transformations between the layers. The coupling of layers with different thicknesses and compositions is advantageous when crack developments is not present. The use of short carbon fibres and a multi-layer structure in a graded composite allows to mitigate the trade-off between the high strength and ablation behaviour, failure tolerance and weight [15,16].

Thanks to their relatively low density, high melting point, high strength and good thermal conductivity, the most studied UHTCs are the ZrB_2-based composites [17–19]. In order to improve the thermo-mechanical properties, oxidation resistance and final density, borides are usually combined with silicon-containing additives in small amount, such as 10–20 vol% of SiC [20,21]. In fact, the oxidation resistance of pure ZrB_2 is poor already at 1000 °C, because of the formation of a porous and non-protective ZrO_2 film, as well as the evaporation of B_2O_3. The introduction of SiC promotes the formation of a surficial glassy silica phase, which protects the material from oxidation up to 1600 °C [22]. Other ceramic additives, such as Y_2O_3 or $MoSi_2$ improve the densification of ZrB_2-SiC composites by forming a liquid phase with the oxide impurities present on the surface of ZrB_2 and SiC grains [23,24]. The presence of Y_2O_3 stabilizes the ZrO_2 formed during oxidation in the tetragonal structure, leading to the formation of a more compact film that improves the oxidation resistance [25]. The presence of $MoSi_2$ improves the oxidation resistance thanks to the formation of a SiO_2 layer. In more detail, oxidation produces a SiO_2-rich glass layer, a subsurface oxide layer, and a MoB, ZrO_2, and SiO_2 mixture layer [26].

In this work, the possibility of producing graded composites with a fibre gradient ranging from 0 to 50 vol% via hot pressing sintering was investigated. Three UHTC matrices were mixed with carbon fibres:

- ZrB_2 – 10 vol% SiC - 5 vol% Y_2O_3 where SiC is the oxidation resistant phase and Y_2O_3 is the sintering aid [4,27].
- ZrB_2 – 15 vol% $MoSi_2$ where $MoSi_2$ is both sintering and oxidation resistant aid [28,29].

* Corresponding author.
E-mail address: antonio.vinci@issmc.cnr.it (A. Vinci).

https://doi.org/10.1016/j.jeurceramsoc.2024.01.099
Received 21 November 2023; Received in revised form 25 January 2024; Accepted 31 January 2024
Available online 3 February 2024

- SiC – 5 vol% Y_2O_3, where Y_2O_3 is the sintering aid [30,31].

The behaviour of the fibres in the different layers and at the interface between the layers after the sintering was examined. Additionally, the oxidation resistance was investigated through tests in air at 1650 °C for one minute, on the top layer and along the cross section, to understand the impact of fibre content on the resistance of reinforced layers vs bulk layers. Indeed, even if in service conditions the underlying fibre-reinforced layers would normally not be exposed to the oxidative environment, it would be interesting to assess the damage in case oxygen broke through the bulk layer during oxidation. Furthermore, the differences in oxidation resistance resulting from the different matrix and sintering aid were investigated.

2. Experimental

2.1. Graded compositions

Three graded materials were manufactured, each with a different matrix composition and varying amounts of pitch-based, short carbon fibre reinforcement. Specifically, a structure consisting of three layers was considered. The first layer consisted solely of bulk ceramic without any reinforcement. The second layer was composed of the same matrix material with a 20 vol% of short fibre reinforcement, and the final layer contained 50 vol% of fibres. The compositions and distribution of fibres in the investigated materials are reported in Table 1.

2.2. Raw materials

The following commercial raw materials were used for the production of the different samples:

1. ZrB_2 (H.C. Starck, grade B, Germany, specific surface area: 1.0 m^2/g, particle size range: 0.5–6 μm, impurities (wt%): 0.25 C, 2 O, 0.25 N, 0.1 Fe, 0.2 Hf);
2. α-SiC (Grade UF-25, H.C. Starck, Germany, specific surface area: 23–26 m^2/g, D50: 0.45 μm, impurities (wt%): 2.5 O);
3. Y_2O_3 (Grade C, H.C Starck, Germany, specific surface area: 10 −16 m^2/g, D50: 0.90 μm, impurities (wt%): 0.005 Al, 0.003 Ca, 0.005 Fe);
4. $MoSi_2$ (Aldrich, Milwaukee, particle size range: 0.5–6 μm, oxygen content: 1 wt%);
5. pitch-based, ultra-high modulus carbon fibres (Granoc Yarn XN80-6 K fibres; tensile modulus of 780 GPa and tensile strength 3.4 GPa, diameter: 10 μm, supplier: Angeloni) manually chopped with a blade to a length of approximately 3 mm;
6. biodegradable thickener used as colloidal dispersant as reported in previous studies

2.3. Process

The fabrication process of the different samples (Fig. 1) was based on a novel approach reported in a previous work [27]. One important characteristic of this process is the ability to overlap sheets with different characteristics - such as the fibre amount - in order to obtain samples with a fibre gradient.

The different powder mixtures were prepared by wet ball milling and drying. Using these mixtures, water-based slurries were prepared and mixed with the dispersant and the desired amount of carbon fibres. The resulting products were then transferred in a mould to be shaped as sheets and dried. The layers were subsequently overlapped to achieve the desired fibre stratification and subjected to debonding in air at mild temperatures. Finally, the layered samples were sintered via hot pressing at 1900 °C for 20 min and 35 MPa of pressure, as reported in previous studies [32–34].

The different samples were each composed of three different regions. The amount of fibre reinforcement for each layer (0 – 20 – 50 vol%, respectively) was chosen to maintain damage tolerance throughout the specimen while also ensuring compatibility between each layer. The bulk layer's thickness was kept as low as possible to guarantee sufficient oxidation resistance without adversely affecting the final weight, while the fraction with 50 vol% fibre content was increased to lower the specific weight and provide high damage tolerance. The coefficients of thermal expansion (CTE) for the materials used are approximately $6.7{\cdot}10^{-6}$/°C for ZrB_2, $4.0{\cdot}10^{-6}$/°C for SiC and $2.0{\cdot}10^{-6}$/°C for the pitch carbon fibres [35,36]. To obtain the final samples, hot pressing was performed on 10 sheets of overlapped material for each composition. Due to the varying amounts of fibres within the layers and the different densities of the matrices, the thickness of each layer was not the same, but the ratio between the layer thicknesses was maintained at 4:7:10 to ensure a good overall compatibility.

2.4. Microstructure analysis

The microstructure was analysed on polished surfaces before and after the oxidation tests using a field emission scanning electron microscope (FE-SEM, Carl Zeiss Sigma NTS Gmbh Öberkochen, Germany) and energy dispersive X-ray spectroscopy (EDS, INCA Energy 300, Oxford instruments, UK). The samples to be analysed with the microscope were prepared by cutting cross sections, mounting them in epoxy resin, and then polishing down to a 0.25 μm finish with diamond abrasives and a using semi-automatic polishing machine (Tegramin-25, Struers, Italy). The polished samples were subsequently washed with ethanol in an ultrasonic bath, dried under IR light, and cleaned with a plasma cleaner (Colibrì Plasma RF 50 kHz, Gambetti, Italy) at 40 W for 5 min with a mixture of argon and 20% oxygen. After sintering, the geometric density and bulk densities were measured. The bulk densities were determined using the Archimedes method with distilled water according to the standard DIN EN 1389:2003.

2.5. Oxidation tests

Oxidation tests were carried out in a bottom-up loading furnace (FC18–0311281, Nannetti S.R.L, Italy). This furnace allows for testing the oxidation and thermal shock resistance of materials directly exposed to the target temperature (e.g. 1650 °C). The furnace can be heated to the desired test temperature, and then the samples are introduced in the chamber. This method ensures a quick exposition to high temperature, bypassing potential oxidation phenomena that could occur at lower temperatures, more closely replicating the typical operating times that are in the order of few seconds and up to 2 min. In this study, samples with approximate dimensions of 5 × 10 × 3 mm (width × length × thickness) were tested at 1650 °C in air for 1 min. Once the target temperature was reached, the samples were placed in the furnace using a porous zirconia sample holder. After reaching thermal equilibrium (approximately 2 min), the isothermal stage began (1 min). At the end of the oxidation test, the samples were quickly removed and allowed to cool naturally in air. The samples were weighed both before (w_{in}) and after (w_{fin}) the oxidation test. The mass variation was normalized over

Table 1
List of the samples tested, relative compositions, additives roles and final density of the graded structures.

Name	Matrix composition (vol %)	Function	ρ (g/cm^2)
ZSY	85 - ZrB_2 10 - SiC 5 - Y_2O_3	ZrB_2: main phase SiC: oxidation resistance aid Y_2O_3: sintering aid	4.30
ZM	85 - ZrB_2 15 - $MoSi_2$	ZrB_2: main phase $MoSi_2$: oxidation and sintering aid	4.85
SY	95 - SiC 5 - Y_2O_3	SiC: main phase Y_2O_3: sintering aid	2.71

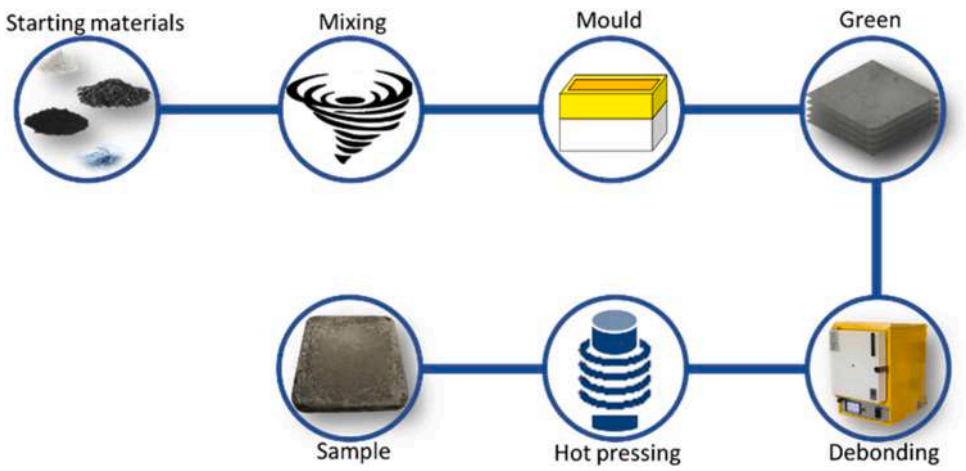

Fig. 1. Flowchart for the fabrication process: the starting materials are mixed, then cast into a mould to obtain fibre-powder sheets, then undergo debonding in air, and finally they are sintered via hot pressing [27].

the initial surface area (S) using the following equation: $\frac{\Delta m}{S} = \frac{w_{fin} - w_{in}}{S}$.

3. Results and discussion

3.1. Microstructural features of the as-sintered graded samples

All graded structures shared similar features: the regions with 0 – 20 – 50 vol% fibres could be clearly identified by SEM, but within each composition, the individual sheets could not be distinguished as they were welded during the sintering process. No fibre aggregation or voids were observed and the outer bulk material was entirely free of cracks, even in proximity of the interface with the fibre-reinforced layers without incurring in CTE-related issues between the layers, as often observed in previous reports [37]. Details of each structure are reported below.

3.1.1. ZSY structure

All the layers were almost fully dense, despite the increasing content of carbon fibres. According to EDS (Fig. 3-**a**) the matrix contained ZrB_2, (light grey phase), SiC (black phase), and ZrC particles. Additionally, dark grey phases of Y-B-C-O were observed, exhibiting a lamellar structure. These Y-B-C-O phases were formed through the reduction of impurities, Y_2O_3 and B_2O_3, with the carbon from the fibres [4,38–40].

The fibres did not show signs of degradation or reaction with the matrix, maintaining their rounded shape (Fig. 2), except for the first ≈ 100 μm of the second layer in the area directly in contact with the first layer. In the region at the interface between the first and second layer,

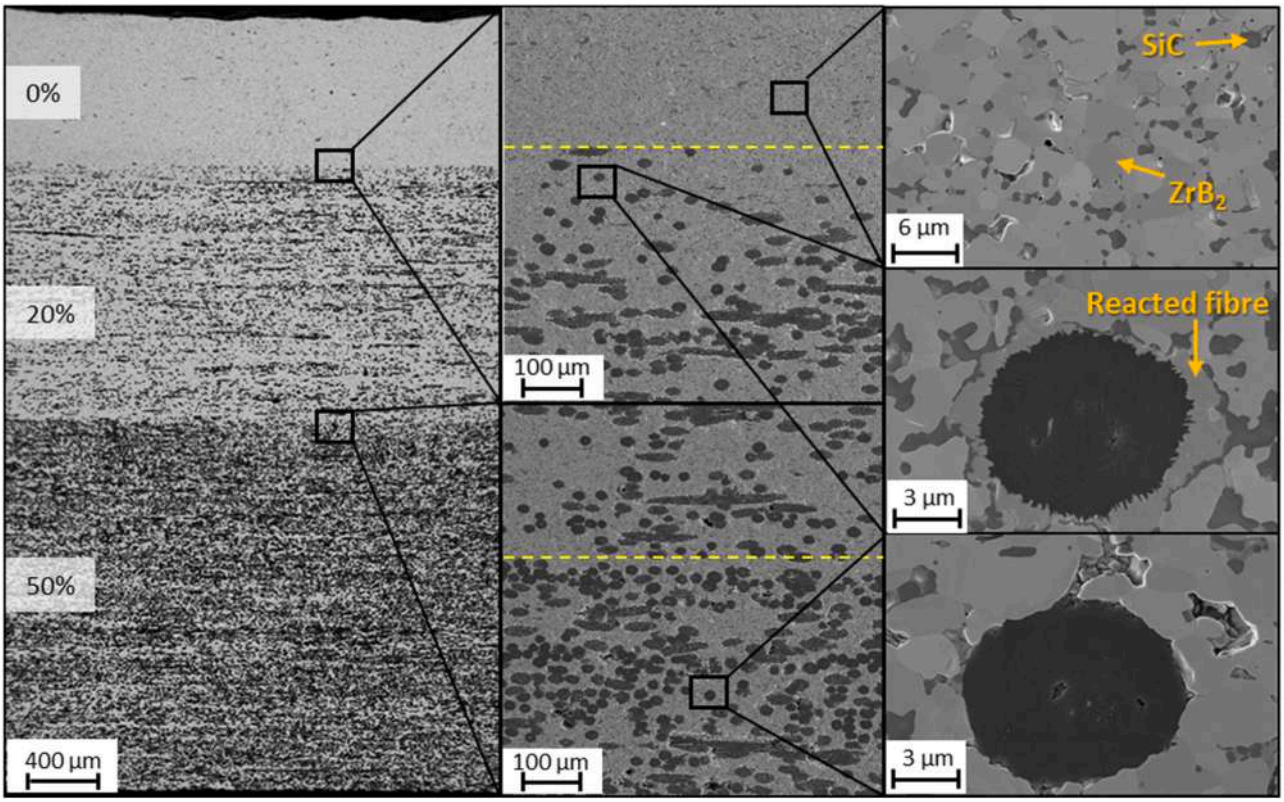

Fig. 2. Morphologies of graded ZSY structure composed of three areas: 0 - 20 - 50 vol% Cf. Thickness of the layers are ~800, 1400, 2000 μm, respectively.

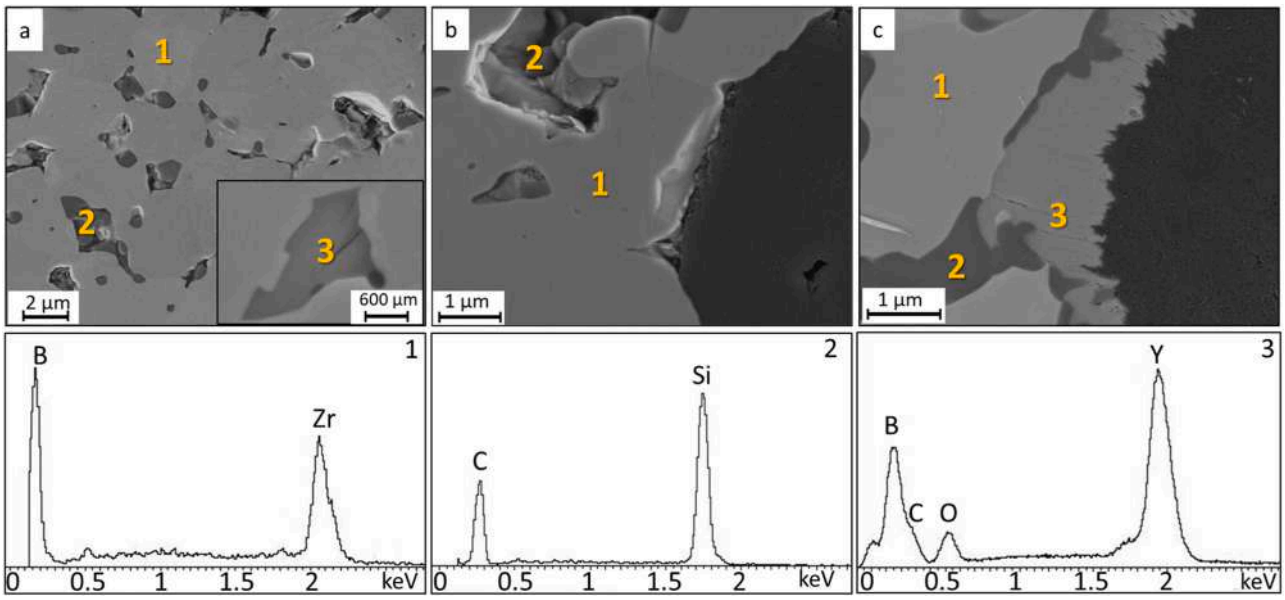

Fig. 3. High magnification SEM images of ZSY sample: (a) matrix (b) unreacted fibre (c) reacted fibre and EDS spectra collected at 5 KeV. The light and dark grey phases represent ZrB_2 (1) and SiC (2) respectively. Occasionally, Y-B-C-O phases (3) were observed near SiC particles.

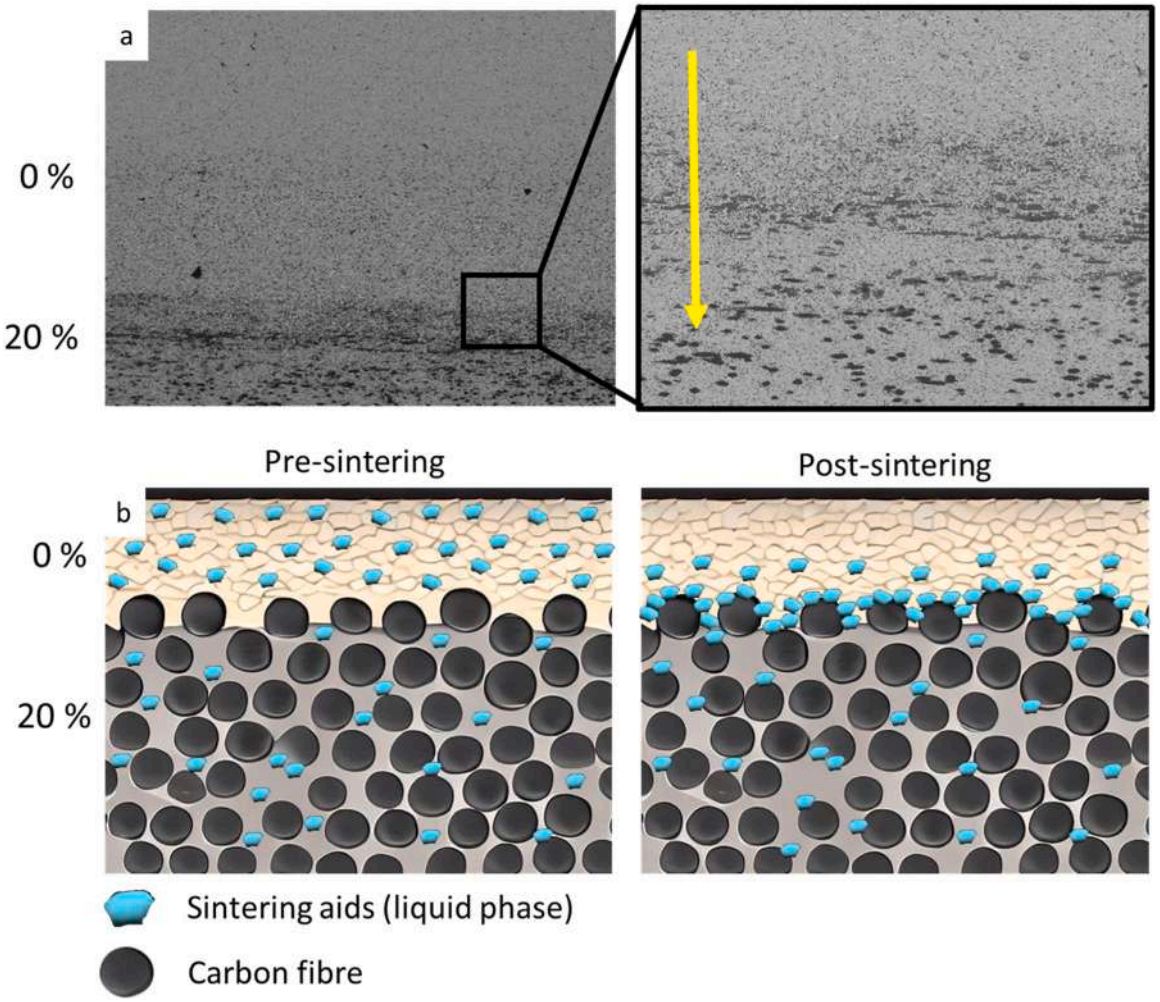

Fig. 4. Detail of the migration of the liquid phase from the bulk layer to the 20% fibre reinforced layer: a) low and high magnification of the interface, showing the gradual impoverishment of the bulk layer of the liquid phase that accumulates near the interface, b) Schematic representation of the migration of the liquid phases during the sintering and the relative fibres reaction.

called the transition zone, the fibres were characterized by radial degradation (Fig. 2) which was confirmed to be Y-B-C-containing phases (Fig. 3-**c**). The hypothesized reaction is reported below [41]:

$$Y_2O_{3(s)} + 2\ B_2O_{3(s)} + 13\ C \rightarrow 2\ YB_2C_{2(s)} + 9\ CO_{(g)}$$

The B_2O_3 mentioned in the reaction came from the oxides naturally covering the surface of the commercial ZrB_2 powder. This reaction was particularly evident only in the fibres at the interface between the first and second layers (Fig. 2). This is likely due to the migration of Y_2O_3 during sintering from the bulk region to the fibres. The migration occurred throughout the material because Y_2O_3, mixed with B_2O_3 and SiO_2, acted as a liquid phase during sintering.

This migration (schematically reported in Fig. 4) was driven by the concentration gradient of the liquid phase that reacted with the carbon fibres reducing its concentration at the interface between the layers.

3.1.2. ZM structure

The surface of the first layer (Fig. 5) was completely dense and homogeneous, without voids or defects. Partially degraded fibres were only observed at the interface between the 0% and 20% fibre reinforced layers, in a region approximately 50 μm thick; in this transition layer, the fibres reacted with the additives, leading to evident fibre degradation.

The EDS spectra collected on the ZrB_2 - $MoSi_2$ matrix (Fig. 6-**a**) revealed the presence of a light grey phase, likely Mo-B, a darker grey phase corresponding to ZrB_2 and a black phase representing SiC. The formation of MoB has been observed in previous studies of similar bulk systems and it was attributed to the reaction between $MoSi_2$ and oxygen impurities during the sintering process [29]:

$$2\ MoSi_2 + \tfrac{5}{2}\ O_2 + B_2O_3 \rightarrow 2\ MoB + 4\ SiO_2$$

EDS analysis performed on the degraded fibres (Fig. 6-**c**) revealed a high concentration of SiC surrounding the fibre, which could be attributed to the reduction of $MoSi_2$ and ZrB_2 with the fibre according to the following reaction:

$$ZrB_{2(s)} + 2\ MoSi_{2(s)} + 5\ C_{(s)} \rightarrow ZrC_{(s)} + 2\ MoB_{(s)} + 4\ SiC_{(s)}$$

The phenomenon of fibre degradation in the transition layer was likely due to the migration of the $MoSi_2$ liquid phase from the bulk area towards the fibres during the sintering process, with the same mechanism observed for the sample ZSY.

3.1.3. SY structure

The addition of Y_2O_3 served as a sintering aid, reducing the sintering temperatures and generating a liquid phase to minimize porosity [31]. This composition was selected after several tests to prevent cracks formation in the matrix caused by residual stresses during sintering. The thickness of each layer was approximately 2.5 mm, 3.9 mm and 4.1 mm, respectively. SEM micrographs on the cross-section (Fig. 7) clearly showed the linear and clear separation between the layers and no cracks were visible on the sample surface. The only critical defect identified was the presence of some voids propagating within the third layer, caused by local fibres agglomeration, leading to a weak interface and the pull-out of fibre bundles (Fig. 7).

The surface microstructure was homogeneous and crack free (Fig. 8-**a**), but exhibited some porosity due to incomplete sintering. The EDS analysis carried out in this area revealed the presence of a dark grey SiC phase and a light grey Y_2O_3 phase.

As for the previous cases, partially degraded fibres were found only in the transition layer that was just 50 μm thick. In this region, the fibres were visibly eroded, but unlike the previous specimens, they were surrounded by voids (Fig. 8-**c**) and the EDS analysis only showed the presence of SiC. Always in this region, a high concentration of a white phase (Y_2O_3) was detected at the interface between the layers, indicating the migration of Y_2O_3 (Fig. 8-**d**).

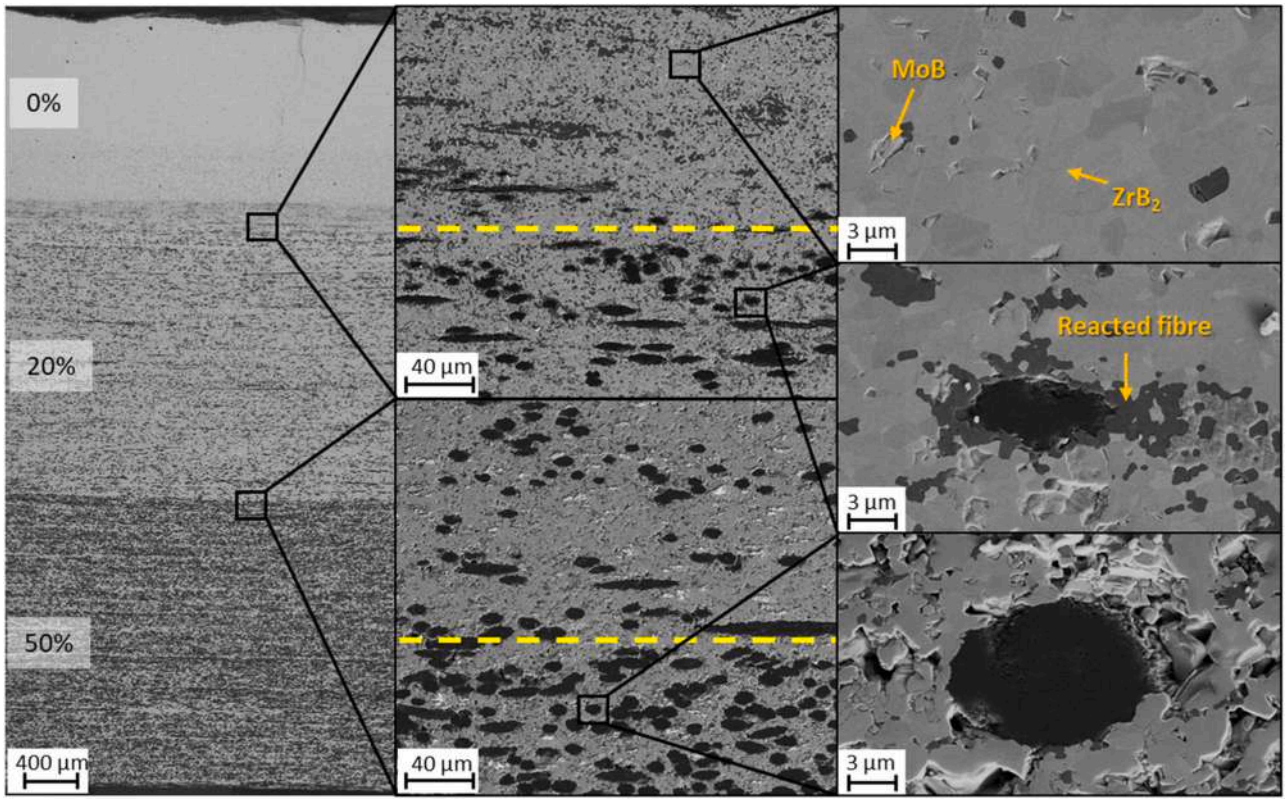

Fig. 5. Morphologies of graded ZM structure composed by three layers: 0 vol%, 20 vol%, 50 vol% of Cf, with thickness of 1.45–2.05-2.10 mm respectively. Yellow lines delineated the transition layer between layers. At the interface between 1st and 2nd areas are visible a pronounced fibres degradation.

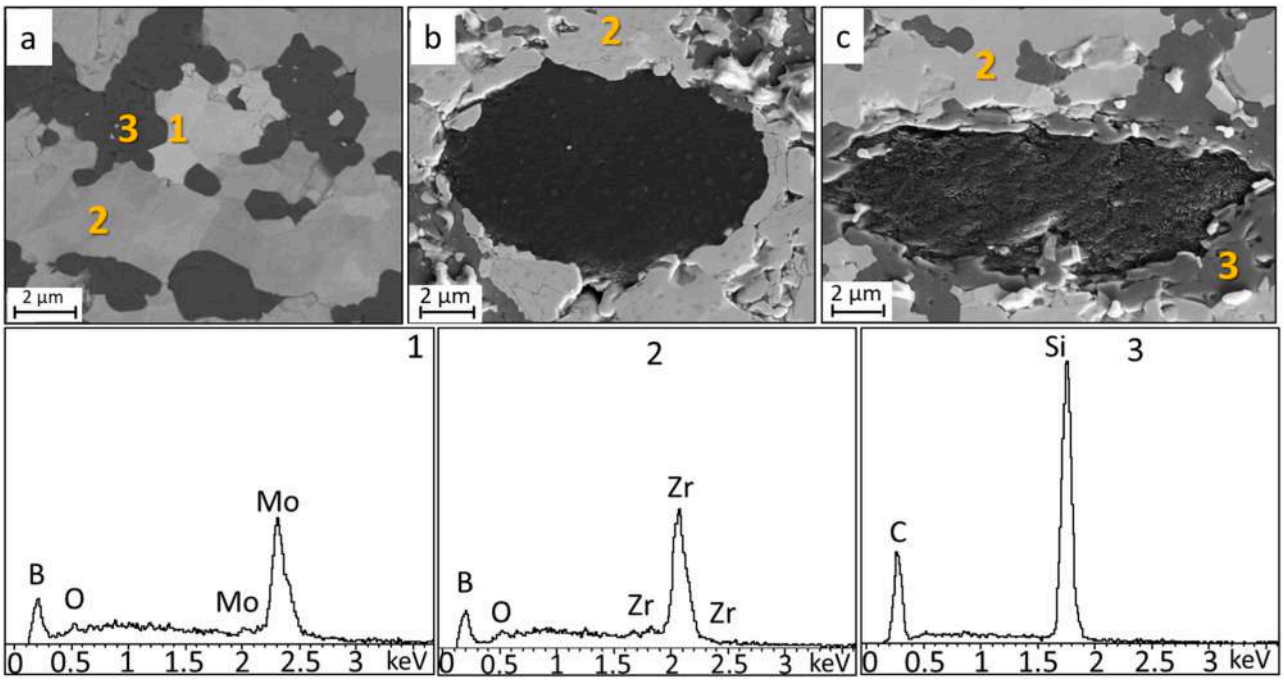

Fig. 6. High magnification SEM images of ZM sample: (a) matrix (b) unreacted fibre (c) reacted fibre and EDS spectra collected at 5 keV. The light grey phase represents MoB (1) and ZrB_2 (2), the darker grey phase corresponds to SiC (3) and black phase represent C.

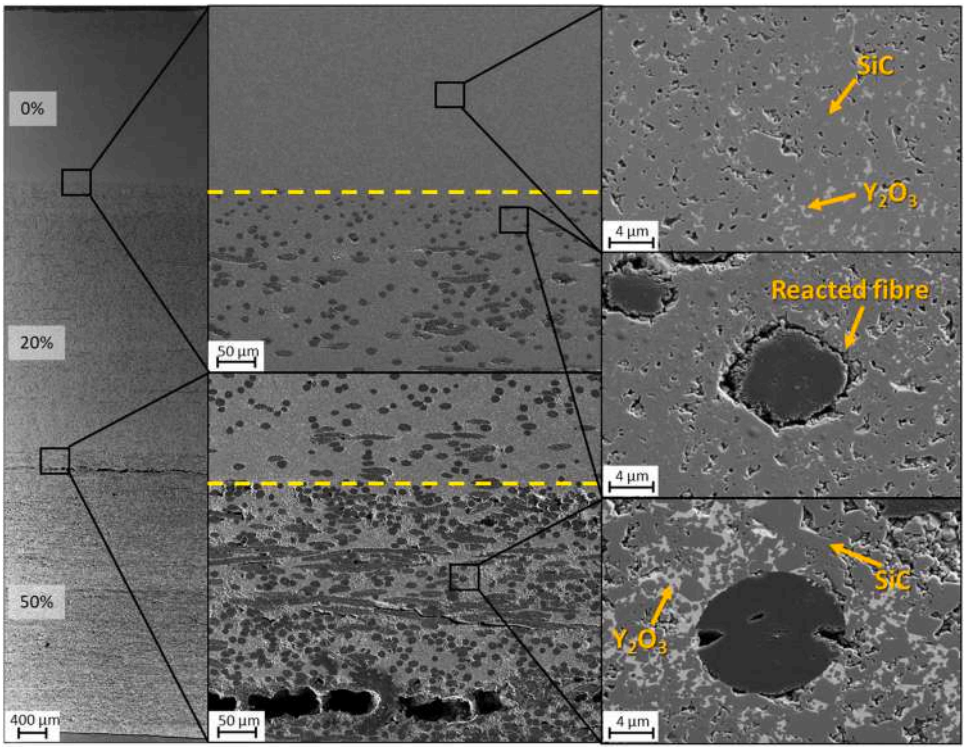

Fig. 7. Morphologies of graded SY structure composed of three areas: 0 vol%, 20 vol%, 50 vol% of Cf. The transition areas between layers are indicated by yellow lines.

3.2. *Microstructural features of the oxidized samples*

Weight changes, mass variation per unit area, and oxidized layer thickness are summarized in Table 2. The lowest weight loss was observed for sample ZM (approximately 0.56 mg/cm^2), as the decrease in weight caused by fibre oxidation was partially compensated by the weight increase due to the oxidation of ZrB_2 to ZrO_2. Sample ZSY exhibited an intermediate mass loss of approximately 4.51 mg/cm^2, in accordance with previous studies on long carbon fibre reinforced ZrB_2-SiC materials [42]. Finally, sample SY showed the highest mass loss of approximately 7.05 mg/cm^2, but at the same time the bulk layer was characterized by the lowest oxide thickness. This phenomenon was

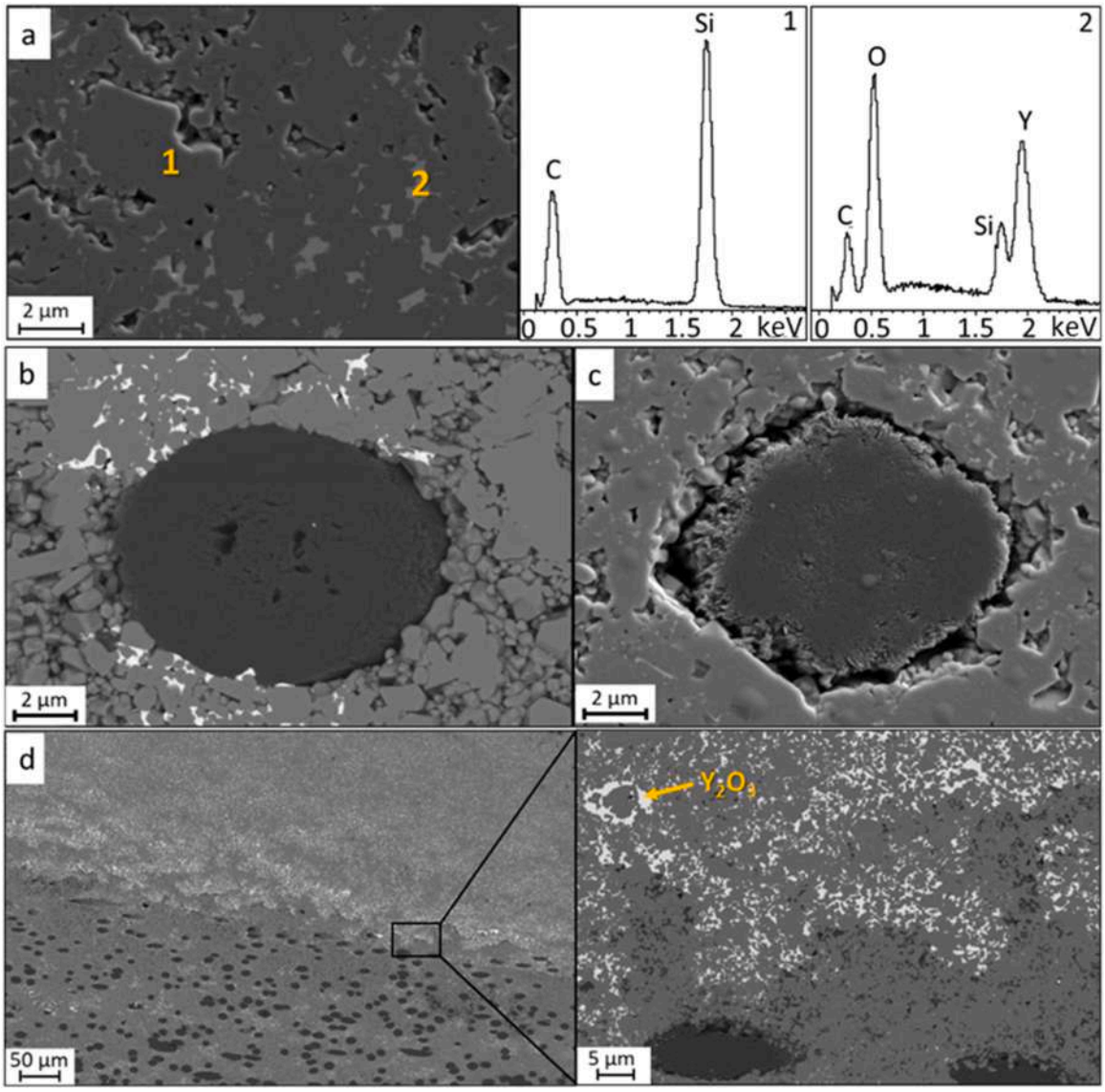

Fig. 8. High magnification SEM image of SY sample: (a) matrix surface and EDS spectra collected at 5 keV, (b) fibre shapes and the relative degree of reaction in all the sample, (c) fibres degradation at the interface between first and second layer, (d), migration and accumulation of Y_2O_3–rich phase (white) at the interface between the first and second layer.

Table 2
Values of mass variation, mass variation per unit area, and layer oxide thickness for the different samples.

	ZSY	ZM	SY
Δm (%)	- 1.34	- 0.14	- 3.46
Δm/S (mg/cm^2)	- 4.51	- 0.56	- 7.05
1st layer ox. thickness (µm)	70 ± 6	50 ± 7	2 ± 1
2nd layer ox. thickness (µm)	120 ± 9	100 ± 9	140 ± 15
3rd layer ox. thickness (µm)	190 ± 16	85 ± 7	230 ± 20

probably due to the absence of mass gain during oxidation.

All the tested samples exhibited high oxidation resistance, in accordance with previous works on similar ceramic matrices reported in literature [43–45]. The presence of varying amounts of carbon fibres in the samples allowed to analyse different structures under oxidation simultaneously.

After the oxidation tests at 1650 °C, the surface and polished cross-section of the graded specimen were examined using SEM. Only the cross-section corresponding to the outer layer (0 vol% Cf) is relevant for the desired application, as the inner layers with higher fibre content would typically not be exposed to air. However, for comparison purposes, the oxidation of the inner layers on the lateral surface was also investigated in this study, to demonstrate how the fibre content would affect the composite's oxidation resistance.

To investigate more in detail the effects of oxidation on the different layers constituting the samples, EDS mapping was carried out. This technique allowed to measure the oxide thickness in each layer, indicated by the red oxygen signal. In all the samples analysed, a gradual increase in thickness of the oxidized area was observed from top to bottom (Table 2). Generally, across all the samples, the oxygen distribution approximately corresponded to changes in matrix morphologies, and variation in oxygen penetration aligned with the interfaces between the different layers.

3.2.1. *ZSY oxidized structure*

3.2.1.1. Oxidized surfaces. The oxidation behaviour of carbon fibre reinforced ZrB_2-SiC-Y_2O_3 material has been previously investigated by the same authors and was used as reference material [4]. The four main

reactions observed were:

$$C_{(s)} + 1/2\ O_{2(g)} \rightarrow CO_{(g)} \quad (1)$$

$$C_{(s)} + O_{2(g)} \rightarrow CO_{2(g)} \quad (2)$$

$$ZrB_{2(s)} + 5/2O_{2(g)} \rightarrow ZrO_{2(s)} + B_2O_{3(l,g)} \quad (3)$$

$$SiC_{(s)} + 3/2\ O_{2(g)} \rightarrow SiO_{2(l)} + CO_{(g)} \quad (4)$$

SEM analysis carried out on sample ZSY after oxidation (Fig. 9-**a**) did not reveal any newly-formed cracks between the layers, suggesting that the difference in CTE between the layers and the thermal shock after cooling down from 1650 °C did not significantly affect the structural integrity of the material. The surface of the first layer was mainly characterized by the presence of bubbles and structures resembling "four-leaves clovers" composed of ZrO_2 (white phase) and SiO_2 (dark grey phase) (Fig. 9-**a**), along with hemispherical structures composed of a very fine layer of ZrO_2.

The second layer with 20 vol% of carbon fibres showed a high concentration of porosity generated by the oxidation of the fibres. In this area, the matrix had a higher amount of SiO_2 on the surface, visible as a dark grey phase. The third layer, reinforced with 50 vol% of carbon fibres, exhibited a higher degree of porosity on the surface due to the higher amount of carbon fibre oxidation and the resulting matrix was predominantly composed of ZrO_2 as evidenced by the distribution of the white phase/ indicating that this high fibre content strongly affected the oxidation resistance. The surface morphology of ZrO_2 was different than that of C-ZrB_2/SiC composites where ZrO_2 is typically present in the form of needles (secondary zirconia) [42], but the cross section revealed the typical columnar growth of ZrO_2. From XRD analysis previously carried out on Y_2O_3-doped composites, no other ZrO_2 phase was observed other than the monoclinic, which could be due to Y_2O_3 no longer being available as oxide but being present as YBCO phases that have different reactivity [46].

3.2.1.2. Polished cross section. The EDS analysis carried out on the polished bulk area (Fig. 9-**c**) revealed the presence of a SiO_2 phase (dark grey/black), a ZrO_2 phase (light grey), and a Y-Si-O-containing phase (grey), likely yttrium silicate.

The oxidation behaviour of the different layers was influenced by the volume content of carbon fibre, as shown in Fig. 9-**b**. Starting from the bulk layer, the oxide scale thickness progressively grows going from 70 μm (0% fibres), to 120 μm (20% fibres) and to 190 μm (50% fibres), highlighting how a graded structure is optimal for the improved protection of UHTCMCs. Previous studies [47,48] have reported that for the ZrB_2-SiC-Y_2O_3 matrix, only one oxidized region is visible, consisting of ZrO_2 grains bound together by a glassy phase of SiO_2 and Y-O. This glassy phase was more abundant near the surface where the oxidation was more pronounced. In the bulk region, columnar ZrO_2 grains, SiO_2 and a few Y-O phases were observed (Fig. 9-**c**). The presence of C in all the spectra was due to the carbon layer deposited by sputtering on the sample for SEM observation. The presence of Y_2O_3 inhibited the formation of the typical two-region structure composed of an outer silica layer and an intermediate scale of columnar $ZrO_2 + SiO_2$, as observed in ZrB_2-SiC matrix composites [42]. The second layer (20% fibres) was characterized by a similar structure, but with the presence of some voids due to the oxidation of the outer fibres. The third layer (50% fibres) was visibly more damaged due to the higher carbon content, with the formation of large voids and of an irregular oxide scale.

3.2.2. ZM oxidized structure

3.2.2.1. Oxidized surface. The entire sample surface (Fig. 10) was covered by a continuous dark grey layer that prevented the identification of any micro or macro defects. This layer was composed of SiO_2, which formed during the oxidation of $MoSi_2$ according to the following reaction:

$$ZrB_{2(s)} + 2MoSi_{2(s)} + 5\ O_{2(g)} \rightarrow ZrO_{2(s)} + 4SiO_{2(s)} + 2MoB_{(s)} \quad (5)$$

All three layers displayed similar features and were mainly constituted by ZrO_2 grains covered by a SiO_2 film (Fig. 10-**a**). With increasing the carbon fibre content, the silica on the surface increased and the amount of visible ZrO_2 grains decreased. Moreover, some porosity was

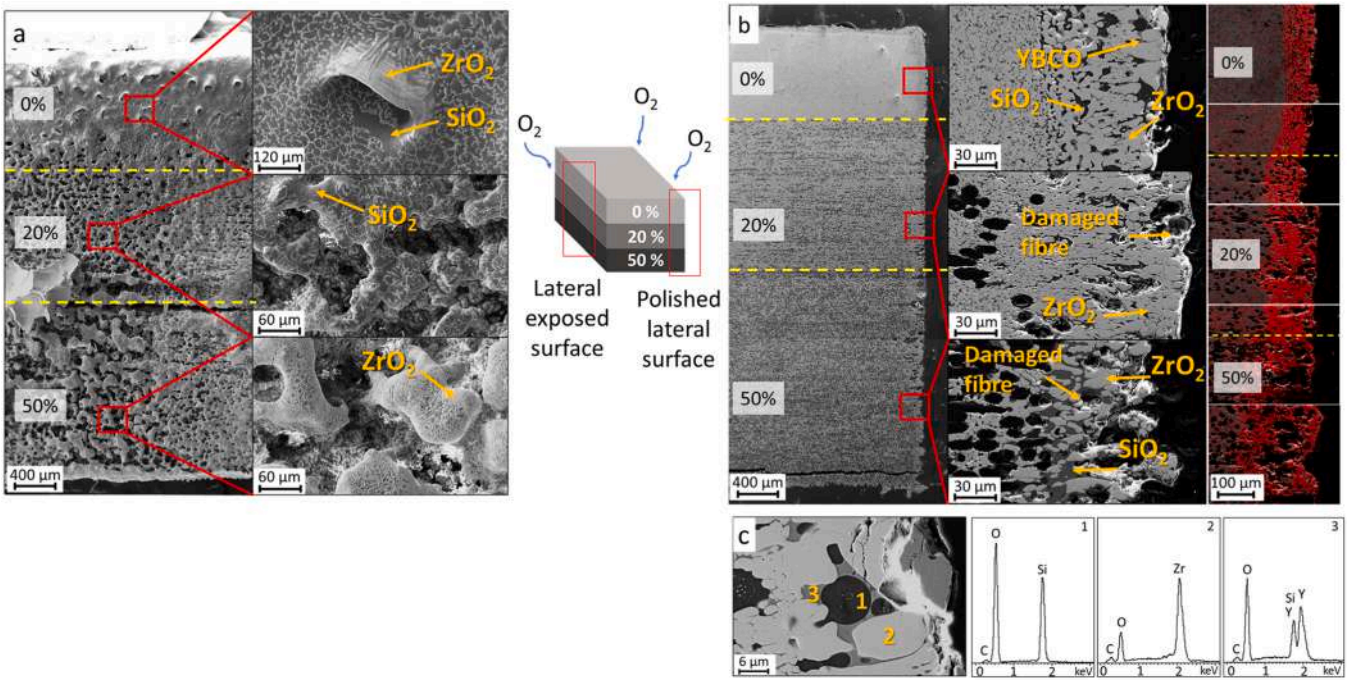

Fig. 9. Morphologies of graded ZSY structure after oxidation at 1650 °C in air: (a) lateral exposed surface, (b) polished lateral surface with EDS mapping (oxygen signal in red, (c) EDS spectra collected at 5 keV of the polished bulk area. The dark grey phases represent SiO_2 (1), the light grey phases are ZrO_2 (2) and the grey phases are yttrium silicates (3).

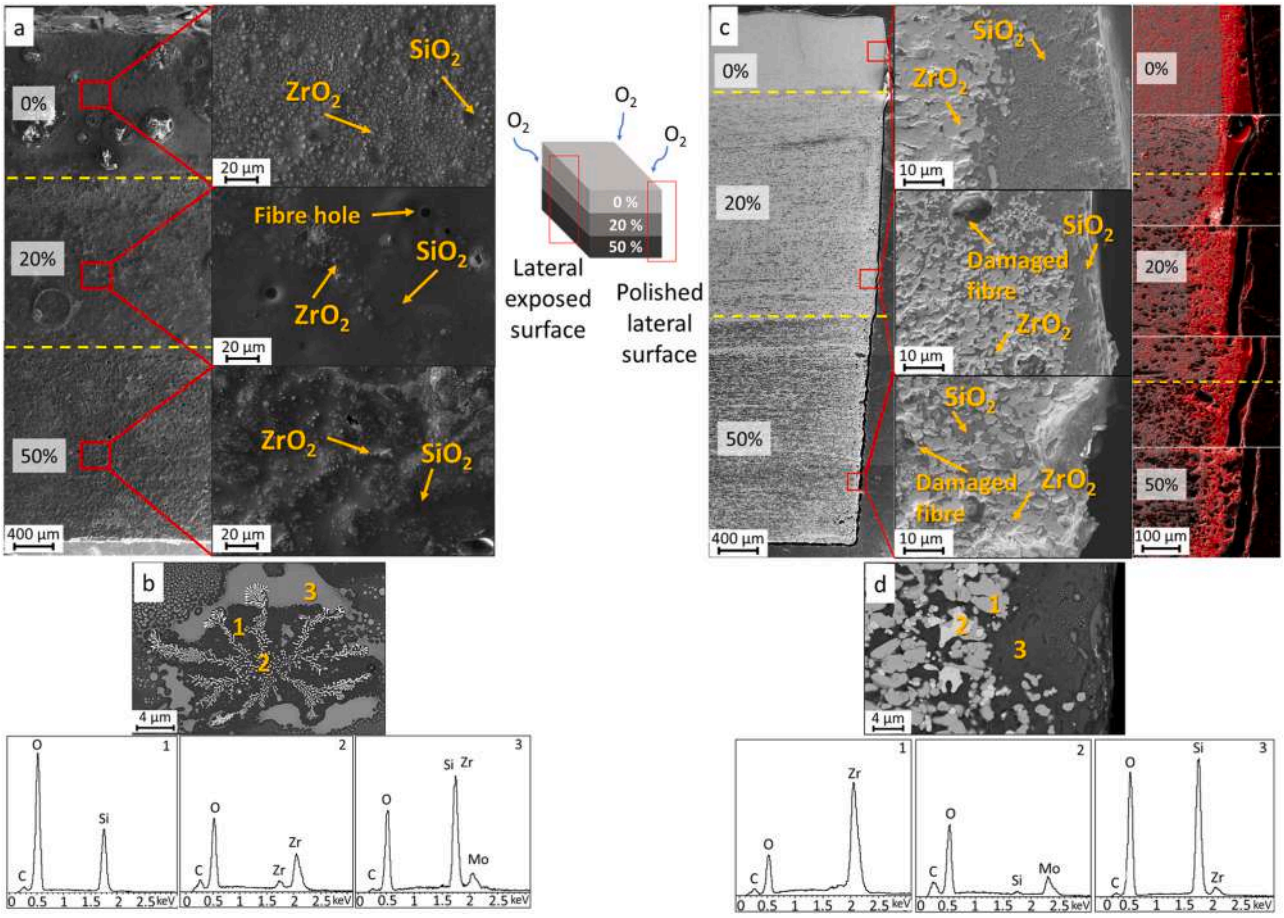

Fig. 10. Morphologies of graded ZM structure after oxidation at 1650 °C in air: lateral exposed surface (a), EDS spectra collected at 5 keV of the bulk area after the oxidation (b), polished lateral surface with EDS mapping (oxygen signal in red) (c) and EDS spectra collected at 5 keV of the polished bulk area (d).

observed, which likely arose from the evolution of CO below the surface due to the oxidation of the outermost fibres. The last layer (50% fibres) was characterized by a less smooth surface, with several bumps and smaller holes, which were attributed to the higher content of carbon oxidation leading to severe bubbling of oxides below the silica layer. Three main phases were identified with EDS (Fig. 10-**b**): a black SiO_2 phase, a white ZrO_2 phase, and a grey phase attributed to MoO_3.

3.2.2.2. Polished cross section. The polished cross-section of sample ZM is reported in Fig. 10-**c**. Upon closer examination, it was evident that no cracks were present in the interfacial regions between the layers, even after the oxidation test. Additionally, the varying degrees of oxidation resulting from the difference in carbon fibre volume in the three layers were clearly visible. In the first layer, a modified region with a thickness of approximately 85 µm was observed. The matrix exhibited a two-region structure following oxidation: an outer SiO_2 film that reduced the oxygen diffusion and an inner ZrO_2 structure. Furthermore, the ZrO_2 grains displayed a well-defined columnar structure held together by a glassy phase of SiO_2.

The second layer, reinforced with 20 vol% of short carbon fibres, showed a modified region with a thickness of approximately 75 µm and displayed the same composition and structure as the previous layer. However, in this layer the outer edge showed some damage due to fibre oxidation. The fibres exhibited a lower degree of oxidation compared to the oxidized ZSY sample, likely due to the enhanced protection provided by the SiO_2 film. In the third layer, reinforced with 50 vol% of carbon fibres, fibre oxidation was observed in an area with a thickness of around 75 µm. However, in this case the protective SiO_2 film was very thin, leading to significant oxidation of the carbon fibres and deformation of the outer profile.

The matrix composition of the polished bulk layer after oxidation, along with the corresponding EDS spectra, is reported in Fig. 10-**d**. The EDS analysis revealed a light grey ZrO_2 phase, resulting from the oxidation of ZrB_2, a white MoO_3 phase, derived from the oxidation of $MoSi_2$, and a dark grey SiO_2 phase, also derived from the oxidation of $MoSi_2$:

$$MoSi_{2(s)} + 3{\cdot}5\ O_{2(g)} \rightarrow MoO_{3(g,l)} + 2SiO_{2(s)} \quad (6)$$

3.2.3. SY oxidized structure

3.2.3.1. Oxidized surfaces. The surface of the cross section of sample SY after oxidation at 1650 °C is reported in Fig. 11-**a**. No newly formed cracks were observed at the interface between the different layers after oxidation, indicating that the CTE mismatch between the layers did not affect the structural integrity. The surface was coated with a dark grey film composed of SiO_2 which formed as a result of the oxidation of SiC according to reaction (4):

In the first layer, a homogeneous dark grey SiO_2 film covered the entire sample. Within this film, lamellar Y_2O_3 phases were observed. The surface did not exhibit any visible defect or bubbles. In the second layer (20% fibres) the SiO_2 film was still visible but without the presence of lamellar Y_2O_3 grains. Moreover, some porosity was observed, likely due to fibre oxidation which left some voids behind that were not covered by the SiO_2 like in the previous two specimens. This behaviour was more evident in the third layer (50% fibres), where the SiO_2 covered the entire area but left a higher number of visible holes due to the fibre oxidation.

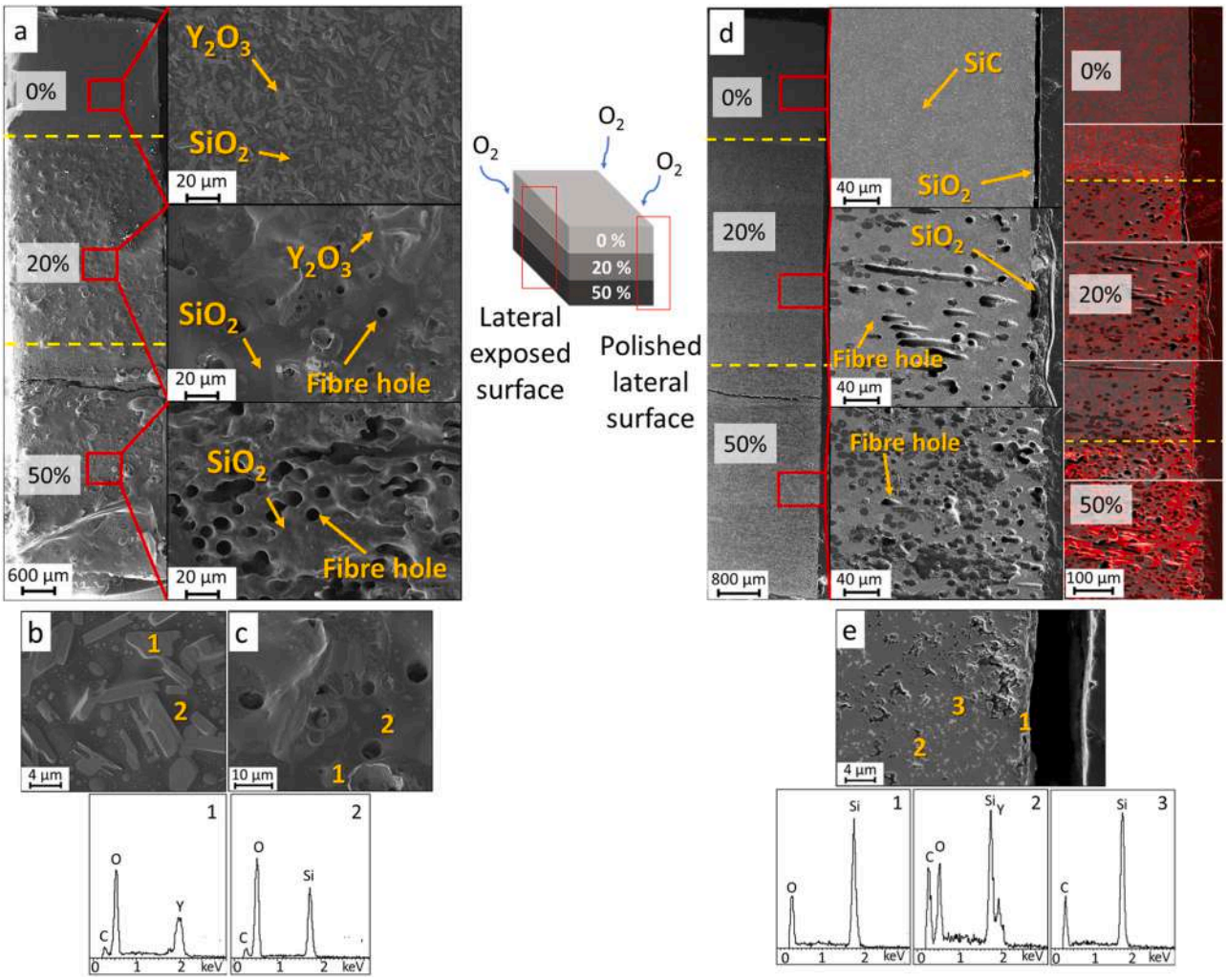

Fig. 11. Morphologies of graded SY structure after oxidation at 1650 °C in air: lateral exposed surface (a), EDS spectra collected at 5 keV of the bulk area after the oxidation (b), EDS spectra collected at 5 keV of the second layer after the oxidation (c), polished lateral surface with EDS mapping (oxygen signal in red) (d) and EDS spectra collected at 5 keV of the polished bulk area (e).

This suggested that the SiO_2 film generated during SiC oxidation does not possess the passivating and protecting properties of the SiO_2 formed in the previous specimens, likely due to insufficient mobility of the oxide and concurrent reactions between the SiO_2 and the SiC substrate and the production of SiO.

The EDS spectra collected on the surface oxide layer revealed the same composition for all three layers but with different distributions. In the first layer (Fig. 11-**b**), light grey Y_2O_3 grains were immersed in a dark grey SiO_2 phase. In the layers reinforced with fibres (Fig. 11-**c**), the elongated Y_2O_3 grains were not present, likely due to the porosity resulting from carbon oxidation, which hindered grain growth.

3.2.3.2. Polished cross section. The polished cross-section of sample SY is shown in Fig. 11-**d**. The polished surface confirmed the absence of cracks in the interface regions between the layers, even after the oxidation test. In the first layer, the SiC matrix appeared mostly unaffected, without significant grain growth or formation of new structures. The second layer (20% fibres), was characterized by a SiO_2 film on the outer surface with a thickness of approximately 220 µm, but the internal SiC matrix was unchanged.

However, numerous holes resulting from the carbon fibres oxidation were visible in the internal region. These holes created a preferential path for oxygen, leading to increased oxygen penetration and a progressively thicker oxide scale going from 140 µm (20% fibres) to 210 µm (50% fibres). Moreover, the external edge showed severe damages due to material loss caused by the formation of cracks between the holes left from the oxidized fibres. These phenomena contributed to increase porosity, which could potentially decrease the mechanical properties of the material.

The EDS spectra collected on the polished bulk layer after the test at 1650 °C (Fig. 11-**e**), revealed the presence of three distinct phases: two different grey phases that identified as SiC and SiO_2, and a light grey phase composed by Y_2O_3.

3.3. Oxidized structure comparison: effect of the matrix composition

By comparing the results obtained for the sample ZSY and ZM, it was possible to investigate the effects of the different additives, namely SiC-Y_2O_3 and $MoSi_2$, respectively. Due to the different nature of the matrix materials and the simultaneous occurrence of mass gain and mass loss phenomena, it was not possible to directly compare the mass loss of the three samples. In the ZrB_2-based samples, the mass loss was partially counterbalanced by the formation of heavier solid oxides, while SiC oxidation mostly led to mass loss. EDS mapping analysis of the first layer revealed oxygen penetration depths of 70 µm for sample ZSY and 50 µm for sample ZM. In the layers below, the oxygen penetration reached depths of 120–190 µm for the second and third layers in sample ZS, while for ZM it was 100–85 µm for second and third layers, respectively.

These variations in oxygen penetration depth suggest that $MoSi_2$ provided better oxidation resistance compared to SiC-Y_2O_3. This could be attributed to the efficacy of $MoSi_2$ to produce a dense and compact silica layer that is compatible with the oxidation products of the boride matrix. The difference in mass loss can also be ascribed to $MoSi_2$ forming solid oxides, whereas the oxidation of SiC leads to the formation of gaseous products like CO. From the Gibbs free energy curves of the oxidation reactions, it can be noted that below 1500 °C the oxidation of the boride matrix is the thermodynamically favoured event even with respect to the oxidation of carbon, suggesting that during the heating up stage, the ZrB_2 matrix of sample ZSY and ZSM is more rapidly oxidised to ZrO_2 and B_2O_3, allowing the formation of a protective scale that slows down the oxidation of the fibres even at 1650 °C, where the latter is more favoured. The presence of $MoSi_2$ further enables the oxidation of ZrB_2 and promotes the early formation of SiO_2, which forms eutectic mixtures with B_2O_3 with lower melting points. The presence of Y_2O_3 can also lead to the formation of yttrium silicates, such as $Y_2Si_2O_7$, whose free energy of formation is negative in the investigated temperature range but higher than the other reactions.

The SiC matrix showed minimal oxygen penetration of approximately 2 μm in sample SY. This difference in oxygen penetration, and hence oxidation resistance, can be attributed to the excellent oxidation resistance provided by SiC at temperatures below 1600 °C [49]. This is in agreement with thermodynamics data shown in Fig. 12, where the oxidation of SiC is among the least favoured oxidation reactions when compared to ZrB_2. Therefore, the SiC matrix appeared to be a better choice as the bulk layer for our oxidation conditions. However, in the second and third layers, the SiC-based composite showed oxygen penetration depth of 140 μm and 210 μm, respectively, considerably higher than ZSY and ZM, highlighting how the similar reactivity of SiC and carbon, coupled with the formation of gaseous oxidation products, leads to an overall inefficient protection; moreover, the lack of other oxides that could form lower melting eutectics leads to the formation of SiO2 with very poor mobility that is unable to cover the voids left by the fibres oxidation.

4. Conclusions

Functionally graded ceramics composed by ZrB_2-SiC-Y_2O_3, ZrB_2-$MoSi_2$ and SiC-Y_2O_3 with a varying carbon fibre content (0–20-50%) were designed to enhance oxidation resistance on the outer layer while minimizing the final density.

All the investigated samples exhibited defect-free interfaces without any cracks within or between the different layers in spite of CTE mismatch of the phases across the sample. In all specimens, the partial migration of the liquid phase was observed from the bulk layer to the 20% fibre reinforced layer, which led to the partial degradation of fibres in this region. However, this did not negatively affect the structural integrity of the material.

The three-layered structure allowed for simultaneous investigation of three different oxidation behaviours in each sample. The oxidation tests conducted at 1650 °C did not result in the formation of cracks or spallation phenomena, demonstrating the good interaction between the different layers. $MoSi_2$ was found as the most effective in protecting the material from oxidation, both in the bulk layer and in the fibre-reinforced layers below, thanks to the formation of a compact SiO_2 scale, showing how even in the event of damage to the outer layer and oxygen penetration to the layers below, the material is still protected. Sample ZSY was characterized by similar performance, but the oxide scale was progressively thicker with the increase of fibre content, while sample SY offered protection only in the most external bulk layer, while the underlying fibre-reinforced layers were completely unprotected.

From the results of this work, graded structures offer the best compromise to retain high oxidation resistance on the exposed outer layer, while maintaining structural integrity and mechanical performance in the layers below and minimizing the specific weight of the material. Even in the event of damage to the outer layer, no spallation or detachment between the different scales occurs thanks to the compatibility between each layer and the high thermal shock resistance. Future studies will be focused on finding the optimal ratio between the individual layers and a full mechanical characterization.

CRediT authorship contribution statement

Matteo Mor: Conceptualization, Methodology, Validation, Investigation, Resources, Writing – original draft; **Antonio Vinci**: Investigation, Visualization, Data curation, Writing – review & editing; **Diletta Sciti**: Writing – review & editing, Supervision, Project administration, Funding acquisition,

Declaration of Competing Interest

The authors declare that they have no known competing financial interests or personal relationships that could have appeared to influence

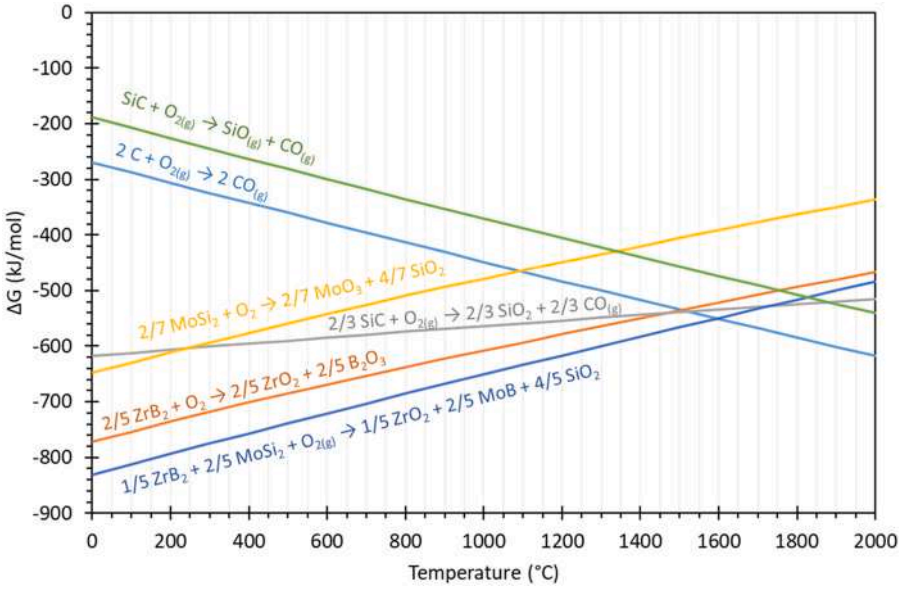

Fig. 12. Gibbs free energy curves for the oxidation reactions 1 – 6, normalised with respect to O_2.

the work reported in this paper.

Data availability

The raw/processed data required to reproduce these findings cannot be shared at this time due to technical or time limitations.

Acknowledgements

This work has received funding from the project CARBOSPACE - "Ultra-refractory Ceramic Composites for Aerospace, Defence, Transport and Energy" (DCM.AD006.251), and from ECOSISTER: Project funded under the National Recovery and Resilience Plan (NRRP), Mission 04 Component 2 Investment 1.5 – NextGenerationEU, Call for tender n. 3277 dated 30/12/2021, Award Number: 0001052 dated 23/06/2022.

References

[1] W.G. Fahrenholtz, G.E. Hilmas, Oxidation of ultra-high temperature transition metal diboride ceramics, Int. Mater. Rev. 57 (2012) 61–72, https://doi.org/10.1179/1743280411Y.0000000012.
[2] D. Ni, Y. Cheng, J. Zhang, J.X. Liu, J. Zou, B. Chen, H. Wu, H. Li, S. Dong, J. Han, X. Zhang, Q. Fu, G.J. Zhang, Advances in ultra-high temperature ceramics, composites, and coatings, J. Adv. Ceram. 11 (2022) 1–56, https://doi.org/10.1007/s40145-021-0550-6.
[3] S.R. Levine, E.J. Opila, M.C. Halbig, J.D. Kiser, M. Singh, J.A. Salem, Evaluation of ultra-high temperature ceramics foraeropropulsion use, J. Eur. Ceram. Soc. 22 (2002) 2757–2767, https://doi.org/10.1016/S0955-2219(02)00140-1.
[4] A. Vinci, L. Zoli, P. Galizia, D. Sciti, Influence of Y2O3 addition on the mechanical and oxidation behaviour of carbon fibre reinforced ZrB2/SiC composites, J. Eur. Ceram. Soc. 40 (2020) 5067–5075, https://doi.org/10.1016/j.jeurceramsoc.2020.06.043.
[5] Z. Balak, M. Zakeri, M. Rahimipour, E. Salahi, Taguchi design and hardness optimization of ZrB2-based composites reinforced with chopped carbon fiber and different additives and prepared by SPS, J. Alloy. Compd. 639 (2015) 617–625, https://doi.org/10.1016/j.jallcom.2015.03.131.
[6] F. Yang, X. Zhang, J. Han, S. Du, Characterization of hot-pressed short carbon fiber reinforced ZrB2-SiC ultra-high temperature ceramic composites, J. Alloy. Compd. 472 (2009) 395–399, https://doi.org/10.1016/j.jallcom.2008.04.092.
[7] Z. Nasiri, M. Mashhadi, A. Abdollahi, Effect of short carbon fiber addition on pressureless densification and mechanical properties of ZrB2-SiC-Csf nanocomposite, Int. J. Refract. Met. Hard Mater. 51 (2015) 216–223, https://doi.org/10.1016/j.ijrmhm.2015.04.005.
[8] S. Mungiguerra, G.D. Di Martino, R. Savino, L. Zoli, L. Silvestroni, D. Sciti, Characterization of novel ceramic composites for rocket nozzles in high-temperature harsh environments, Int. J. Heat. Mass Transf. 163 (2020) 120492, https://doi.org/10.1016/J.IJHEATMASSTRANSFER.2020.120492.
[9] L. Silvestroni, E. Landi, K. Bejtka, A. Chiodoni, D. Sciti, Oxidation behavior and kinetics of ZrB2 containing SiC chopped fibers, J. Eur. Ceram. Soc. 35 (2015) 4377–4387, https://doi.org/10.1016/J.JEURCERAMSOC.2015.07.024.
[10] L. Silvestroni, L. Pienti, S. Guicciardi, D. Sciti, Strength and toughness: the challenging case of TaC-based composites, Compos. Part B: Eng. 72 (2015) 10–20, https://doi.org/10.1016/J.COMPOSITESB.2014.11.043.
[11] L. Silvestroni, D. Pavan, C. Melandri, D. Sciti, N. Gilli, L. Ortiz-Membrado, E. Jiménez-Piqué, A.M. Grande, Functionally graded ultra-high temperature ceramics: From thermo-elastic numerical analysis to damage tolerant composites, Mater. Des. 224 (2022) 111379, https://doi.org/10.1016/J.MATDES.2022.111379.
[12] R. Bermejo, Y. Torres, A.J. Sánchez-Herencia, C. Baudín, M. Anglada, L. Llanes, Residual stresses, strength and toughness of laminates with different layer thickness ratios, Acta Mater. 54 (2006) 4745–4757, https://doi.org/10.1016/J.ACTAMAT.2006.06.008.
[13] N.A. Orlovskaya, J. Kuebler, V.I. Subotin, M. Lugovy, High toughness ceramic laminates by design of residual stresses, MRS Online Proc. Libr. (OPL) 702 (2001) U8.7.1, https://doi.org/10.1557/PROC-702-U8.7.1.
[14] L. Náhlík, L. Šestáková, P. Hutař, R. Bermejo, Prediction of crack propagation in layered ceramics with strong interfaces, Eng. Fract. Mech. 77 (2010) 2192–2199, https://doi.org/10.1016/J.ENGFRACMECH.2010.02.023.
[15] L. Silvestroni, C. Melandri, V. Venkatachalam, J. Binner, D. Sciti, Merging toughness and oxidation resistance in a light ZrB2 composite, Mater. Des. 183 (2019) 108078, https://doi.org/10.1016/j.matdes.2019.108078.
[16] L. Silvestroni, C. Capiani, D. Dalle Fabbriche, C. Melandri, Novel light and tough ZrB2-based functionally graded ceramics, Compos. Part B: Eng. 99 (2016) 321–329, https://doi.org/10.1016/J.COMPOSITESB.2016.06.001.
[17] P. Hu, W. Guolin, Z. Wang, Oxidation mechanism and resistance of ZrB2-SiC composites, Corros. Sci. 51 (2009) 2724–2732, https://doi.org/10.1016/j.corsci.2009.07.005.
[18] W. Li, X. Zhang, C. Hong, J. Han, W. Han, Hot-pressed ZrB2-SiC-YSZ composites with various yttria content: microstructure and mechanical properties, Mater. Sci. Eng. A 494 (2008) 147–152, https://doi.org/10.1016/j.msea.2008.04.010.
[19] R.V. Krishnarao, V.V. Bhanuprasad, G. Madhusudhan Reddy, ZrB2–SiC based composites for thermal protection by reaction sintering of ZrO2+B4C+Si, J. Adv. Ceram. 6 (2017) 320–329, https://doi.org/10.1007/s40145-017-0244-2.
[20] K. Shugart, S. Liu, F. Craven, E. Opila, Determination of retained B2O3 content in ZrB2-30 vol% SiC oxide scales, J. Am. Ceram. Soc. 98 (2015) 287–295, https://doi.org/10.1111/JACE.13236.
[21] P.A. Williams, R. Sakidja, J.H. Perepezko, P. Ritt, Oxidation of ZrB2–SiC ultra-high temperature composites over a wide range of SiC content, J. Eur. Ceram. Soc. 32 (2012) 3875–3883, https://doi.org/10.1016/J.JEURCERAMSOC.2012.05.021.
[22] A. Vinci, L. Zoli, P. Galizia, D. Sciti, Influence of Y2O3 addition on the mechanical and oxidation behaviour of carbon fibre reinforced ZrB2/SiC composites, J. Eur. Ceram. Soc. 40 (2020) 5067–5075, https://doi.org/10.1016/j.jeurceramsoc.2020.06.043.
[23] X. Zhang, X. Li, J. Han, W. Han, C. Hong, Effects of Y2O3 on microstructure and mechanical properties of ZrB2-SiC ceramics, J. Alloy. Compd. 465 (2008) 506–511, https://doi.org/10.1016/j.jallcom.2007.10.137.
[24] W.M. Guo, J. Vleugels, G.J. Zhang, P.L. Wang, O. Van der Biest, Effects of Re2O3 (Re = La, Nd, Y and Yb) addition in hot-pressed ZrB2-SiC ceramics, J. Eur. Ceram. Soc. 29 (2009) 3063–3068, https://doi.org/10.1016/j.jeurceramsoc.2009.04.021.
[25] W. Li, X. Zhang, C. Hong, J. Han, W. Han, Hot-pressed ZrB2-SiC-YSZ composites with various yttria content: microstructure and mechanical properties, Mater. Sci. Eng. A 494 (2008) 147–152, https://doi.org/10.1016/j.msea.2008.04.010.
[26] D. Sciti, M. Brach, A. Bellosi, Oxidation behavior of a pressureless sintered ZrB2–MoSi2 ceramic composite, J. Mater. Res. 20 (2005) 922–930, https://doi.org/10.1557/JMR.2005.0111.
[27] M. Mor, A. Vinci, S. Failla, P. Galizia, L. Zoli, D. Sciti, A novel approach for manufacturing of layered, ultra-refractory composites using pliable, short fibre-reinforced ceramic sheets, J. Adv. Ceram. 12 (2023) 155–168, https://doi.org/10.26599/JAC.2023.9220674.
[28] D. Sciti, M. Brach, A. Bellosi, Oxidation behavior of a pressureless sintered ZrB2–MoSi2 ceramic composite, J. Mater. Res. 20 (2005) 922–930, https://doi.org/10.1557/JMR.2005.0111.
[29] D. Sciti, S. Guicciardi, A. Bellosi, G. Pezzotti, Properties of a pressureless-sintered ZrB2–MoSi2 ceramic composite, J. Am. Ceram. Soc. 89 (2006) 2320–2322, https://doi.org/10.1111/J.1551-2916.2006.00999.X.
[30] E. Gomez, J. Echeberria, I. Iturriza, F. Castro, Liquid phase sintering of SiC with additions of Y2O3, Al2O3 and SiO2, J. Eur. Ceram. Soc. 24 (2004) 2895–2903, https://doi.org/10.1016/j.jeurceramsoc.2003.09.002.
[31] S. Ding, S. Zhu, Y. Zeng, D. Jiang, Effect of Y2O3 addition on the properties of reaction-bonded porous SiC ceramics, Ceram. Int. 32 (2006) 461–466, https://doi.org/10.1016/j.ceramint.2005.03.024.
[32] D. Sciti, A. Natali Murri, V. Medri, L. Zoli, Continuous C fibre composites with a porous ZrB2 Matrix, Mater. Des. 85 (2015) 127–134, https://doi.org/10.1016/j.matdes.2015.06.136.
[33] D. Sciti, P. Galizia, T. Reimer, A. Schoberth, C.F. Gutiérrez-Gonzalez, L. Silvestroni, A. Vinci, L. Zoli, Properties of large scale ultra-high temperature ceramic matrix composites made by filament winding and spark plasma sintering, Compos. Part B: Eng. 216 (2021) 108839, https://doi.org/10.1016/j.compositesb.2021.108839.
[34] D. Sciti, L. Zoli, T. Reimer, A. Vinci, P. Galizia, A systematic approach for horizontal and vertical scale up of sintered Ultra-High Temperature Ceramic Matrix Composites for aerospace – Advances and perspectives, Compos. Part B: Eng. 234 (2022) 109709, https://doi.org/10.1016/J.COMPOSITESB.2022.109709.
[35] P. Galizia, L. Zoli, D. Sciti, Impact of residual stress on thermal damage accumulation, and Young's modulus of fiber-reinforced ultra-high temperature ceramics, Mater. Des. 160 (2018) 803–809, https://doi.org/10.1016/j.matdes.2018.10.019.
[36] W. Lengauer, Transition metal carbides, nitrides, and carbonitrides, Handb. Ceram. Hard Mater. (2008) 202–252, https://doi.org/10.1002/9783527618217.CH7.
[37] F. Servadei, L. Zoli, P. Galizia, A. Vinci, D. Sciti, Development of UHTCMCs via water based ZrB2 powder slurry infiltration and polymer infiltration and pyrolysis, J. Eur. Ceram. Soc. 40 (2020) 5076–5084, https://doi.org/10.1016/j.jeurceramsoc.2020.05.054.
[38] G. Zhao, J. Chen, Y. Li, M. Li, YB2C2: a machinable layered ternary ceramic with excellent damage tolerance, Scr. Mater. 124 (2016) 86–89, https://doi.org/10.1016/j.scriptamat.2016.06.041.
[39] Y. Zhou, H. Xiang, X. Wang, W. Sun, F.Z. Dai, Z. Feng, Electronic structure and mechanical properties of layered compound YB2C2: a promising precursor for making two dimensional (2D) B2C2 nets, J. Mater. Sci. Technol. 33 (2017) 1044–1054, https://doi.org/10.1016/j.jmst.2016.09.028.
[40] A. Vinci, L. Zoli, L. Silvestroni, N. Gilli, D. Sciti, Synthesis, microstructure and mechanical properties of lamellar YB2C2 – based ultra-high temperature ceramic composites, J. Eur. Ceram. Soc. 43 (2023) 831–841, https://doi.org/10.1016/J.JEURCERAMSOC.2022.10.072.
[41] A. Vinci, L. Zoli, P. Galizia, D. Sciti, Influence of Y2O3 addition on the mechanical and oxidation behaviour of carbon fibre reinforced ZrB2/SiC composites, J. Eur. Ceram. Soc. 40 (2020) 5067–5075, https://doi.org/10.1016/j.jeurceramsoc.2020.06.043.
[42] A. Vinci, L. Zoli, D. Sciti, Influence of SiC content on the oxidation of carbon fibre reinforced ZrB2/SiC composites at 1500 and 1650 °C in air, J. Eur. Ceram. Soc. 38 (2018) 3767–3776, https://doi.org/10.1016/j.jeurceramsoc.2018.04.064.
[43] E. Eakins, D.D. Jayaseelan, W.E. Lee, Toward oxidation-resistant ZrB2-SiC ultra high temperature ceramics, Metall. Mater. Trans. A: Phys. Metall. Mater. Sci. 42 (2011) 878–887, https://doi.org/10.1007/S11661-010-0540-8/FIGURES/8.
[44] S.Q. Guo, Densification of ZrB2-based composites and their mechanical and physical properties: a review, J. Eur. Ceram. Soc. 29 (2009) 995–1011, https://doi.org/10.1016/J.JEURCERAMSOC.2008.11.008.

[45] X. Ren, H. Chu, K. Wu, A. Zhang, M. Huang, C. Ma, H. Liu, P. Feng, Effect of the ZrB2 content on the oxygen blocking ability of ZrB2-SiC coating at 1973K, J. Eur. Ceram. Soc. 41 (2021) 1059–1070, https://doi.org/10.1016/J.JEURCERAMSOC.2020.10.036.

[46] A. Vinci, L. Silvestroni, N. Gilli, L. Zoli, D. Sciti, Advancements in carbon fibre reinforced ultra-refractory ceramic composites: effect of rare earth oxides addition, Compos. Part A: Appl. Sci. Manuf. 156 (2022) 106858, https://doi.org/10.1016/j.compositesa.2022.106858.

[47] A. Vinci, L. Zoli, P. Galizia, D. Sciti, Influence of Y2O3 addition on the mechanical and oxidation behaviour of carbon fibre reinforced ZrB2/SiC composites, J. Eur. Ceram. Soc. 40 (2020) 5067–5075, https://doi.org/10.1016/j.jeurceramsoc.2020.06.043.

[48] A. Vinci, L. Zoli, E. Landi, D. Sciti, Oxidation behaviour of a continuous carbon fibre reinforced ZrB2–SiC composite, Corros. Sci. 123 (2017) 129–138, https://doi.org/10.1016/j.corsci.2017.04.012.

[49] A. Kovalčíková, J. Sedláček, Z. Lenčéš, R. Bystrický, J. Dusza, P. Šajgalík, Oxidation resistance of SiC ceramics prepared by different proceessing routes, J. Eur. Ceram. Soc. 36 (2016) 3783–3793, https://doi.org/10.1016/J.JEURCERAMSOC.2016.03.016.